Journal of Applied Polymer Science

Dual drug release from CO_2-infused nanofibers via hydrophobic and hydrophilic interactions

Brett C. Geiger,[1] Mark Tyler Nelson,[1] Hrishikesh R. Munj,[2] David L. Tomasko,[2] John J. Lannutti[3]
[1]Department of Biomedical Engineering, The Ohio State University, Columbus, Ohio 43210
[2]William G. Lowrie Department of Chemical and Biomolecular Engineering, The Ohio State University, Columbus, Ohio 43210
[3]Department of Materials Science and Engineering, The Ohio State University, Columbus, Ohio 43210
Correspondence to: J. J. Lannutti (E-mail: lannutti.1@osu.edu)

ABSTRACT: This study investigated the effects of hydrophobic–hydrophilic interactions on dual drug release from CO_2-infused nanofibers scaffolds (PCL, PCL–gelatin, and PCL "core" PCL–gelatin "shell") using BODIPY 493/503 and Rhodamine B fluorescent dyes as drug models. Favorable dye–scaffold interactions increased total dye loading and promoted steady, more linear release. Unfavorable dye–scaffold interactions reduced overall loading and led to a greater burst release of dye. However, when CO_2 was used to infuse dye into an unfavorable scaffold, the changes in loading and release were less pronounced. When two dyes were infused, these behaviors were accentuated due to interactions between the dissolved forms of the dyes. Core–shell composite nanofibers displayed radically different release properties versus pure PCL–gelatin fibers when treated with dyes via CO_2 infusion. Dye release from core–shell scaffolds was highly sensitive to both interactions with scaffolds and the phase of CO_2 used to infuse the compounds of interest. By using different phases of CO_2 to partition dyes into hydrophobic and hydrophilic sections of core–shell nanofibers, such interactions can be manipulated to develop a bimodal drug release system with potential application in drug delivery or tissue engineering. © 2015 Wiley Periodicals, Inc. J. Appl. Polym. Sci. **2015**, *132*, 42571.

KEYWORDS: adsorption; biodegradable; biomaterials; drug delivery systems; polyesters

Received 17 December 2014; accepted 1 June 2015
DOI: 10.1002/app.42571

INTRODUCTION

Biomimetic materials, both synthetic and natural, have been applied as biomaterials for drug delivery and tissue engineering applications. In early efforts, alginate, a compound derived from seaweed, was used as the basis for wound dressings.[1,2] Other natural polymers including collagen, fibrin, chitosan, and even xenograft dermis have been investigated and utilized for their ability to interact favorably with cells and provide a biological microstructure mimicking the extracellular matrix (ECM) of human tissues.[3–8] In contrast, synthetic polymers have a distinct advantage in that they are easily tailored for a specific application, providing an engineered alternative with control over properties such as modulus, molecular weight, and degradation rate.[9–11] Biocompatible polymers such as polyglycolic acid (PGA), polylactic acid (PLA), polyurethanes (PU), and polycaprolactone (PCL) see widespread use in drug delivery and tissue engineering applications.[9,12–14] However, a shortcoming of these synthetic materials lies in their inherently limited biofunctionality. Electrospinning is a polymer processing technique that has been used to produce nanoscale-diameter fibers from all these synthetics, providing a high-surface-area substrate attractive for regenerative medicine applications as it resembles the microstructure and morphology of native ECM.[9,12–17]

To increase bioactivity, investigators have applied many different techniques of biofunctionalization to electrospun nanofibers including surface coupling of biomolecules and drug infusion into the polymer.[17–21] In particular, controlled release of incorporated drugs is an expanding area of research due to the enormous potential to affect biologic sites via spatiotemporal differences in drug application.[22] Standard approaches to provide this level of control include diffusion barriers, polymer swelling by solvation, chemical degradation, and actuation via external stimuli such as magnetic fields or heat.[21] While in some cases effective, these methods can prove challenging to control and often lead to deleterious effects on nanofiber morphology or drug bioactivity.[23] Supercritical fluids technology utilizes the phase transitions of CO_2 to provide an effective means of drug incorporation and release from nanofiber scaffolds via precise control over pressure and temperature during infusion.[24] Previous studies have established both supercritical and subcritical CO_2 infusion as a benign, green, and inexpensive technique that can be used to biofunctionalize nanofiber scaffolds.[24–26]

In this context, chronic wounds are a specific type of condition that, due to a malfunction in the natural healing process, can take years to heal and in some cases may not heal at all. This results in long-term pain, persistent infection, and lengthy hospitalizations. These wounds affect nearly 6.5 million patients in the United States alone, resulting in a yearly medical expenditure of $25 billion.[27] The biological causes of aberrancy in chronic wounds are quite complex. Therefore, recent engineering approaches to scaffold design for this application frequently incorporate multiple drugs into a single scaffold.[22,28–31] Thus, controlled release has become increasingly important as interactions between these drugs as well as interactions between the drugs and scaffold must be elucidated. Hydrophobic–hydrophilic interactions play a prominent role in diffusion-based release.[21] Several studies have proposed such interactions as a means of controlling release behavior but only a few have investigated and quantified their effects.[29,30,32] To make progress toward the goal of an electrospun nanofiber scaffold having multiple drug functionalization realized by CO_2 infusion, this study aims to investigate the effects that hydrophobic–hydrophilic match and mismatch have on the loading and release of drugs infused into electrospun nanofibers via supercritical or subcritical CO_2 exposure.

Drugs were modeled in this study using two different fluorescent dyes. Rhodamine B ([9-(2-carboxyphenyl)-6-diethylamino-3-xanthenylidene]-diethylammonium chloride) was used as a model hydrophilic drug, while BODIPY 493/503 (4,4-difluoro-1,3,5,7-tetramethyl-4-bora-3a,4a-diaza-s-indacene-8-propionic acid) was utilized as a model hydrophobic drug. PCL was used as a hydrophobic scaffold and a 50 : 50 PCL–gelatin blend as a hydrophilic scaffold. Dyes were infused into each scaffold in a variety of hydrophobicity match–mismatch conditions via supercritical and/or subcritical CO_2 exposure. Adsorptive exposures to the dye solution were used as a control treatment. Both release of dye over a 2-week period and the initial dye loading were used to quantify the effects of dye–scaffold interactions on controlled release. Visual observation of scaffolds before and after release was used to draw qualitative conclusions. Favorable dye–scaffold interactions led to increased dye loading and gradual, linear release. Conversely, the opposite was observed for unfavorable interactions. CO_2 infusion, without changing scaffold microstructure, positively impacted both dye loading and longer-term release when individual dyes were infused into unfavorable scaffolds (e.g. hydrophobic dye, hydrophilic scaffold). Dye release from core–shell scaffolds was highly sensitive to both interactions with scaffolds and the phase of CO_2 used to infuse the compounds of interest. This study aims to improve the understanding of drug–drug and drug–scaffold interactions within an electrospun nanofiber system exhibiting dual infusion and release. This understanding will enable the development of tightly controlled multidrug release from CO_2 infused nanofiber scaffolds to better modulate complex challenges in drug delivery and tissue engineering.

EXPERIMENTAL

Polymer and Dye Solutions

Polycaprolactone (PCL) of 5 wt % (Sigma-Aldrich, St. Louis, MO; Mn 70–90 KDa) and type A porcine gelatin of 6.7 wt % (300 Bloom; Sigma-Aldrich, St. Louis, MO) solutions were produced by dissolution in 1,1,1,3,3,3-hexafluoro-2-propanol (HFP) (Oakwood Chemical, West Columbia, SC) at room temperature (~25°C) for 24 h with magnetic stirring. Initially separate solutions of PCL and gelatin were mixed in equal parts by volume and the combination stirred at room temperature (~25°C) for 24 h to create a hydrophilic blend. Pure PCL solution was used as a hydrophobic polymer. Solutions containing 0.1 mg/mL of Rhodamine B (≥97% purity, Ex: 540 nm, Em: 625 nm; Standard Fluka, Sigma-Aldrich, St. Louis, MO) and 0.1 mg/mL of BODIPY 493/503 (≥99.5% purity, Ex: 493, Em: 503; Life Technologies, Carlsbad, CA) were dissolved separately in 100% ethanol (Hedwin, Baltimore, MD). Dual dye solutions containing both 0.1 mg/mL Rhodamine B and 0.1 mg/mL BODIPY were also produced. Stirring at room temperature for 24 h was necessary to dissolve BODIPY in ethanol solution. Both dye solutions were protected from photobleaching by wrapping the solution containers in aluminum foil and storing them in the dark when not in use.

Electrospinning

Solutions of PCL–gelatin blend and pure PCL were poured into 60 mL syringes, fitted with an 18-gage blunt-tip needle, and mounted onto a syringe pump (kdScientific, Holliston, MA). Solutions were electrospun into 7.5 × 7.5 cm nanofiber scaffolds using a DC high-voltage power supply (Glassman High Voltage, High Bridge, NJ) at 20 kV and a cathode to anode separation of 21 cm.[33] Flow rates and electrospinning time were adjusted to ensure good fiber production, as shown in the SEM, and 10 mL of polymer solution was required to fabricate each scaffold. "Core–shell" nanofibers were produced using a concentric needle attachment wherein PCL solution flowed through the center needle while PCL–gelatin solution flowed through a larger diameter needle surrounding it. The previously listed electrospinning parameters were used for core–shell samples as well. The core-to-shell flow rate ratio was established at 1 : 4. Disc samples of 16 mm diameter were removed from as-produced nanofiber sheets using a metal arc punch (CS Osborn & Co, Harrison, NJ) and weighed. Discs of 20–30 mg were used in this study.

Dye Infusion

All samples were placed on a sheet of aluminum foil in a chemical fume hood. Five hundred microliters of 0.1 mg/mL dye solution was pipetted in 100 μL increments onto the surface of each scaffold to initiate adsorption; 10 min separated each application ensuring that all dye solution was taken up by the sample. The samples were then allowed to dry at room temperature for 24 h in a fume hood before infusion. Control scaffolds were not subjected to infusion, only adsorption as described above. Samples were treated with BODIPY dye alone, Rhodamine B dye alone, or a mixture of BODIPY/Rhodamine B dye solution. Dyes were adsorbed onto the scaffolds and then the scaffolds were exposed to either sub- or supercritical CO_2 infusion conditions. Core–shell samples were treated with either of the two dye solutions independently and infused using two different CO_2-assisted infusion conditions sub-(6.20 MPa, 25°C) and supercritical (8.27, 37°C).

Experimental scaffolds were lightly covered with aluminum foil and inserted into a stainless-steel vessel for CO_2 infusion. CO_2 (Praxair, Columbus, OH) was compressed via a 1015 mL syringe pump (Teledyne ISCO, Lincoln, NE) to high pressures within the vessel. Scaffolds were exposed for 2 h to either subcritical CO_2 at 6.20 MPa at 25°C or supercritical CO_2 at 8.27 MPa at 37°C. After infusion, the vessel was depressurized slowly overnight for approximately 18 h. The temperature was maintained using a thermocouple system incorporated into the pressure vessel apparatus. Upon removal from the vessel, infused as well as adsorbed samples were rinsed using separate 15 mL glass vials containing 70% ethanol for 30 min. Following rinsing, the scaffolds were dried overnight in a laminar-flow fume hood and placed into fresh vials wrapped in aluminum foil. Dye loading was then defined as the amount of dye remaining within the scaffold following this ethanol wash step.

Dye Release

Scaffolds were submerged and fully saturated in 1 mL of phosphate buffered saline (PBS) (AMRESCO, Solon, OH) containing 0.1 wt % sodium azide (Sigma Aldrich, St. Louis, MO). At specified time points over the course of 2 weeks, the PBS was removed from each vial and stored in a 1.5 mL microcentrifuge tubes (FisherBrand, Florence, KY). The PBS removed was replaced with 1 mL of fresh PBS. Aliquots of collected dye samples were placed into 96 well plates (FisherBrand, Florence, KY) and analyzed with a fluorescence spectrophotometer (Spectra Max 190, Sunnyvale, CA), and converted to mass of dye released at each time point using a calibration curve created from serial dye dilutions.

Initial Sample Loading and Dissolution

To quantify the dye remaining in the sample at the conclusion of the release period, each nanofiber scaffold was dissolved in 5 mL of HFP over 72 h following 2 min of initial vortexing (VWR Vortex, VWR International, Radnor, PA). These solutions were then diluted by a factor of 5 in HFP. Aliquots of the diluted solutions were placed into polypropylene 96 well plates (FisherBrand, Florence, KY) and immediately analyzed with a fluorescence spectrophotometer against a calibration curve for the different dyes in HFP for conversion to the mass of dye remaining in each sample post-release. Dye loading was calculated as the total amount of dye released plus the amount of dye remaining in the sample after the release period.

Scanning Electron Microscopy

Morphological changes before and after CO_2 exposure were analyzed using SEM. As-spun samples, subcritical post-infusion samples, and supercritical post-infusion samples were adhered to aluminum studs using carbon tape (Ted Pella, Reading, CA) and sputter-coated under argon gas with a 15 nm layer of Au-Pd (Pelco Model 3 sputter coater 91000, USA) at an emission current of 15 mA. Samples were examined by SEM (Quanta 300, Netherlands) allowing microstructural characterization at an accelerating voltage of 12 kV.

X-ray Diffraction

To measure changes in crystallinity following infusion, X-ray diffraction (XRD) (Ultima III, Rigaku Inc, Japan) utilizing a Cu X-ray source (40 kV) was conducted on samples before and after CO_2 infusion.[34] Punches of 22 mm diameter were removed from as spun PCL and core–shell nanofiber sheets and subjected to XRD analysis. The PCL punch was then subjected to subcritical infusion and the core–shell punch was subjected to supercritical infusion. Both samples were again analyzed using XRD over the range of 20–30° 2θ.

Contact Angle Testing

Scaffold hydrophobicity was analyzed by contact angle measurement. Samples of PCL, PCL–gelatin, and core–shell nanofiber scaffolds were analyzed using a sessile drop method on an Easy Drop goniometer (Kruess, Hamburg, Germany). Deionized water (400 μL) was placed onto the scaffold as a single drop and a screenshot taken after 3 s. Easy Drop software was utilized to calculate a contact angle based on the screenshot. Five measurements were taken for each type of scaffold and averaged.

Image Analysis

Changes in sample color following release were visible to the naked eye. Representative images of PCL and PCL–gelatin infused with both dyes before and after the 2-week release process were taken using a bright field camera.

RESULTS AND DISCUSSION

Scaffold Microstructure

Pressurized CO_2 has recently gained interest within the research realm as a benign, green, and inexpensive technique to swell polymer matrices and embed molecules within them. As such, CO_2 is an attractive vehicle for biomolecule infusion directed toward tissue engineering efforts. Previous studies in our group have shown varying biomolecule infusion and release behavior by modifying the pressure and phase of CO_2.[34] This prior publication concerned the infusion and release of only a single compound—Rhodamine B—into polymer blends. The core–shell fibers that are the primary focus of this study were not considered. Dense subcritical CO_2 provides moderate plasticization, leading to some impregnation of biomolecules beneath the surface of a polymer scaffold, enabling prolonged release. Supercritical CO_2 fully plasticizes the polymer material, embedding molecules deep within the scaffold and enabling steady release.[34] Prior work on our part has shown the mutual solubility of PCL and high pressure CO_2[24]. Additional efforts have established that gelatin is not soluble in the same solvent[34] and these differences drive the ability of the different polymer phases to accommodate the infusion of Rhodamine B or BODIPY.

While microstructural changes during the infusion process are generally reversible, supercritical CO_2 is so effective in swelling certain polymers, such as PCL, that it destroys the nanoscale scaffold morphology, potentially eliminating useful properties that depend on scaffold microstructure.[24,35–40] To prevent this phenomenon from damaging electrospun nanofibers and to preserve their valuable microstructure, PCL can be blended in equal parts with porcine gelatin. Gelatin undergoes dehydration upon exposure to supercritical CO_2 causing it to compress and prevent excessive PCL chain motion that would ordinarily denature nanofiber morphology.[34] SEM imaging was used to observe the nanofibrous microstructure of the electrospun scaffolds, both before and after CO_2 infusion. Figure 1 displays the SEM

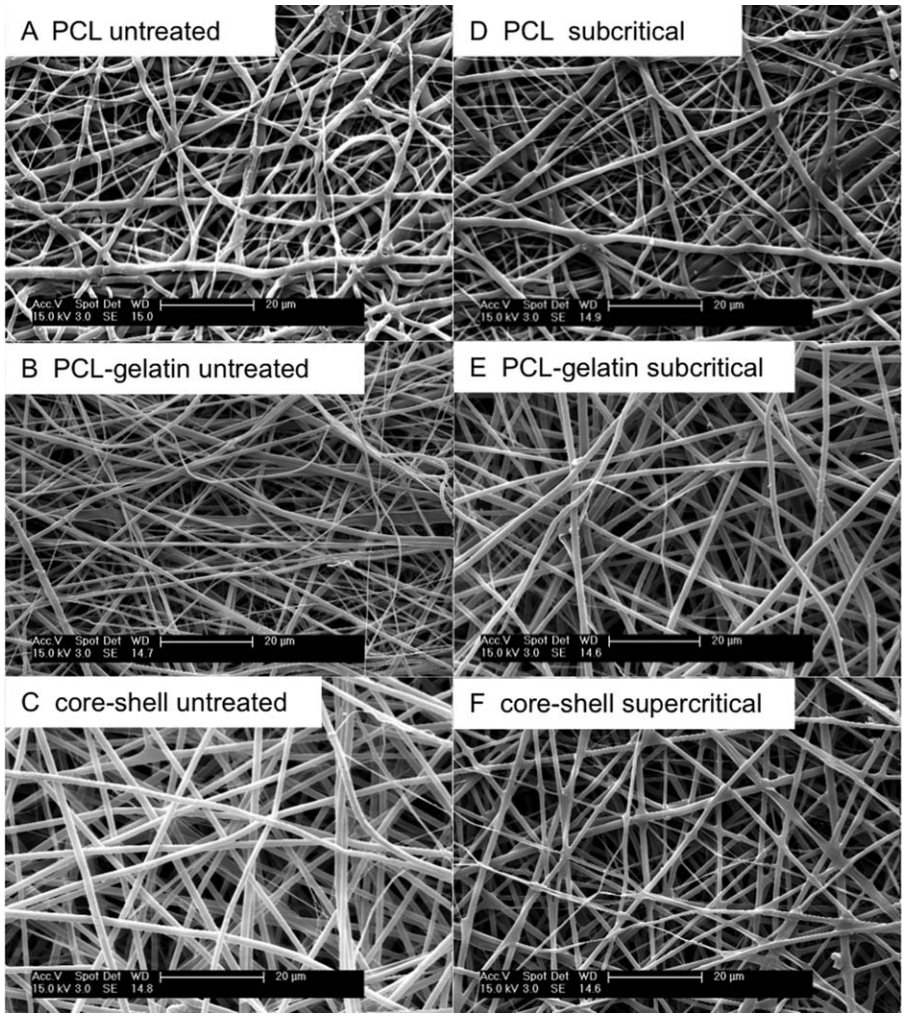

Figure 1. Scanning electron microscope images of (A–C) untreated and (D–F) treated PCL, PCL–gelatin, and PCL "core" PCL–gelatin "shell" nanofiber scaffolds, respectively. PCL and PCL–gelatin scaffolds were treated with subcritical (6.2 MPa, 25°C) CO_2 and core–shell scaffolds were treated with supercritical (8.27 MPa, 37°C) CO_2. All scaffolds retain clear nanofiber morphology after CO_2 exposure.

images of pre- (A–C) and post-CO_2 exposed (D–F) electrospun PCL, PCL–gelatin, and PCL "core" PCL–gelatin "shell" nanofibers. It can be seen that electrospun nanofibers form a dense fibrous matrix closely resembling that of native tissue's extracellular matrix, especially the >80% porosity. Figure 1(A,D) shows as-spun PCL fibers (A) that are uniform, continuous, and free of beads or fiber–fiber bonds. Post-exposure to subcritical CO_2, PCL fibers (D) display minor fiber–fiber bonding without substantial changes to the overall microstructure. PCL–gelatin nanofibers [Figure 1(B,E)] pre- (B) and post-subcritical CO_2 (E) treatment display no significant difference in microstructure or morphology as a result of exposure. Interestingly, PCL "core" PCL–gelatin "shell" nanofibers display intact microstructure and porosity before and after supercritical CO_2 exposure [Figure 1(C,F)], suggesting that the PCL–gelatin shell has enough interaction with the pure PCL core to shield or protect it from supercritical CO_2-driven morphological alteration.

X-ray Diffraction Analysis. X-ray diffraction spectra (Figure 2) further imply that subcritical and supercritical CO_2 exposures do not cause significant alterations in the microstructure of PCL and core–shell nanofiber scaffolds, respectively. PCL and core–shell samples both show only very minor shifts of the characteristic PCL crystal peaks (at 21.5 and 24° 2θ) following infusion. PCL shows the anticipated increases in peak intensity upon exposure to subcritical CO_2, an effect previously attributed to the enhanced mobility of pre-existing aligned yet poorly crystalline PCL chains.[34] Both subcritical and supercritical CO_2 melt (in the polymer physics sense) most of the crystalline regions of polymers before swelling occurs. However, the swelling process increases free volume and chain mobility, allowing crystalline microstructure to reform and grow extensively during slow depressurization, leading to the observed increase in peak intensity for highly crystalline pure PCL. The core–shell fibers have a very low crystallinity because the majority of the fiber, the PCL–gelatin blend, is completely amorphous since the presence of gelatin disrupts PCL crystallization.[34] The pure PCL core contributes some crystallinity but comprises only ~20 vol % of a core–shell fiber.

Contact Angle Testing. Contact angle experiments were used to validate the hypothesis that PCL constitutes a hydrophobic polymer and 50 : 50 PCL–gelatin blend constitutes a hydrophilic

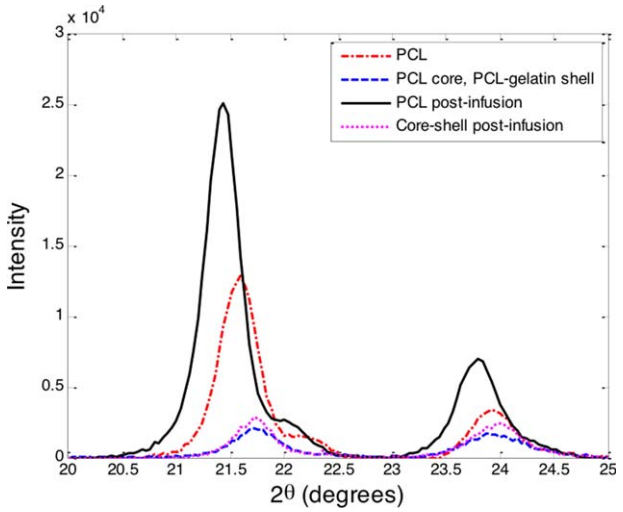

Figure 2. X-ray diffraction data from PCL and PCL "core" PCL–gelatin "shell" fibers pre- and post-infusion. Pure PCL fibers were infused subcritically at 6.20 MPa and 25°C while core–shell fibers were infused supercritically at 8.27 MPa and 37°C. An increase in intensity of characteristic PCL peaks at 21.5 and 24° 2θ post-infusion can be seen. [Color figure can be viewed in the online issue, which is available at wileyonlinelibrary.com.]

polymer. PCL displayed a wetting angle of $126.16 \pm 14.74°$, while PCL–gelatin displayed a wetting angle of 0° immediately after water droplets were placed onto it. By definition, PCL is considered hydrophobic and PCL–gelatin is considered hydrophilic.

Dye Release Behavior

Interactions between drug and scaffold play an important role in drug release kinetics, particularly in diffusion-based systems. While PCL and blended PCL–gelatin are both biodegradable polymers, neither loses an appreciable amount of mass over the release period and therefore release from these scaffolds is governed solely by diffusion. Hydrophobic–hydrophilic interactions are an appealing target for investigation as they can be easily manipulated via appropriate material/drug selection, scaffold plasma treatment, and polymer blending.[41]

Figure 3 displays an optical image of the electrospun nanofiber samples as saturated with equal concentrations of BODIPY and Rhodamine B fluorescent dye before and after release. Both the PCL and PCL–gelatin scaffolds [Figure 3(A,B)] have acquired a similar dark-red color prior to release. Post-release images [Figure 3 (C,D)] display colors representative of the residual dye remaining after 334 h of release. PCL nanofiber scaffolds assume a green-color post-release while PCL–gelatin fibers display an orange-red tint post-release. This difference in color post-release confirms that BODIPY has a high affinity for PCL due to the hydrophobic interactions and that Rhodamine B has a high affinity to PCL–gelatin due to hydrophilic interactions with the gelatin.

Figure 4 displays the percentage of total BODIPY (A) or Rhodamine B (B) released from PCL and from PCL–gelatin nanofiber scaffolds. BODIPY [Figure 4(A)] displays no significant difference in release percentage for simple adsorption-treated PCL or PCL–gelatin scaffolds. However, significant differences in both the release profile and percentage of dye released are observed for nanofiber scaffolds treated with subcritical 6.20 MPa CO_2-assisted infusion. Subcritically infused BODIPY PCL samples release 2.5% of their total loading, while PCL–gelatin releases 3.5%. Release of subcritically infused BODIPY from PCL or PCL–gelatin scaffolds displayed an initial burst release (likely due to residual surface adsorbed dye), followed by linear release kinetics driven by diffusion.

Rhodamine B release from PCL or PCL–gelatin scaffolds (Figure 4(B)) displays significant burst release kinetics for both adsorption and subcritically infused PCL and PCL–gelatin at the early time points. Steady linear release is observed for subcritically infused Rhodamine B-treated samples after 24 h. Adsorbed Rhodamine B exhibited nearly twofold release from PCL scaffolds compared to PCL–gelatin, further illustrating favorable hydrophilic interactions between Rhodamine B and gelatin. No significant difference in the percentage of total Rhodamine B release was observed between adsorption on PCL–gelatin and subcritical infusion on PCL or PCL–gelatin. However, in terms of the total mass of dye released, subcritically infused PCL–gelatin scaffolds released ~9000 ng of dye, statistically greater than all other conditions. Rhodamine B adsorption-treated PCL scaffolds released 84% of its total loaded content within 24 h, while PCL scaffolds treated with Rhodamine B by subcritical infusion released only 45% of their total content over the course of this study. Subcritical infusion was able to mitigate the burst release tendency for unfavorable dye–scaffold interactions.

Figure 5 displays the release of dye from PCL and PCL–gelatin scaffolds exposed to equal concentrations of combined BODIPY + Rhodamine B dye solutions, comparing the results of subcritical CO2 infusion versus simple adsorption. BODIPY [Figure 5(A)] release displays very little difference from that of single dye infusion [Figure 4(A)] in terms of percentage of dye

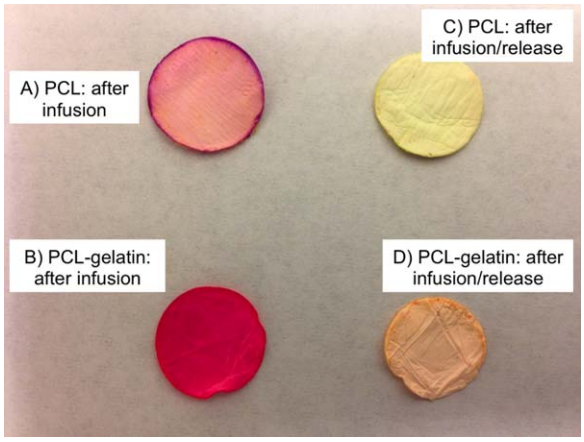

Figure 3. Visual appearance of PCL and PCL–gelatin after (A, B) subcritical CO_2 infusion of BODIPY + Rhodamine B at 6.20 MPa and 25°C and after (C, D) 334 h of release in PBS. Scaffolds both appear red before release. Post-release, PCL adopts the green color of BODIPY dye while PCL–gelatin is predominantly red in color, a characteristic of Rhodamine B dye. [Color figure can be viewed in the online issue, which is available at wileyonlinelibrary.com.]

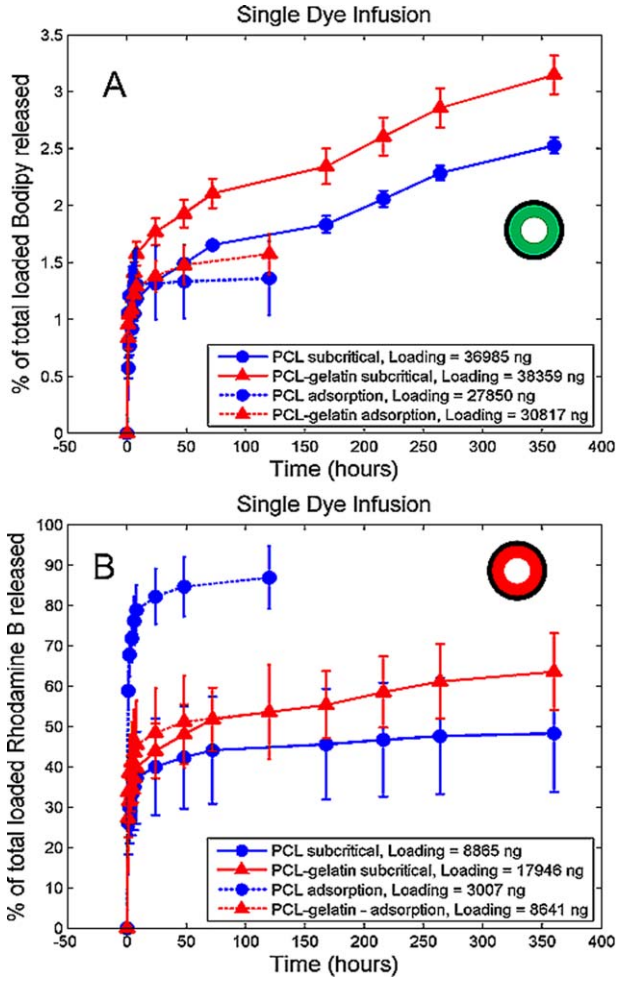

Figure 4. Release of A) BODIPY and B) Rhodamine B represented as a percent of initial scaffold loading following infusion of a single dye into PCL or PCL–gelatin. A representation of expected dye distribution through a fiber cross-section is given as an inset, in which the superficial and deep zones of a fiber are colored according to the following scheme: green, BODIPY; red, Rhodamine B; purple, both dyes; white, no dye. In the schematic, subcritical infusion localizes dye to the superficial zone of the fiber while supercritical infusion localizes dye to both the superficial (shell) and deep (core) zones. Total initial loading in nanograms is also given and is defined as the amount of dye remaining in the scaffold after infusion and a 30-min wash in 70% ethanol. [Color figure can be viewed in the online issue, which is available at wileyonlinelibrary.com.]

released or release profile. However, significant differences are evident in Rhodamine B release when both dyes are present [Figure 5(B)]. The release of subcritically infused Rhodamine B from PCL (unfavorable) increased by 20% over single dye-infused scaffolds, while release of subcritically infused Rhodamine B from PCL–gelatin (favorable) decreased by 40% compared to single dye conditions (Figure 4 (B)). The effects on release of favorable and unfavorable dye–scaffold interactions are exacerbated when two dyes are present and must compete for partitioning within the scaffold during the CO_2 infusion process.[42] In adsorption-treated scaffolds, no significant difference in the percentage of Rhodamine B released was observed between single and dual dye infusion conditions [Figures 4(B) and 5(B)], suggesting that competitive partitioning is induced by CO_2 infusion.

Figure 6(A) shows that within PCL "core" PCL–gelatin "shell" scaffolds, supercritical infusion of BODIPY releases dye more slowly compared to BODIPY infused under subcritical conditions. This trend is opposite that for Rhodamine B-infused scaffolds, displaying increased release percentages for supercritically infused scaffolds as compared to subcritically infused nanofiber scaffolds. It is expected, as shown in the figure inset, that supercritical CO_2 localizes dye throughout the entire fiber while subcritical CO_2 only localizes the dye near the outside of the fiber. For both BODIPY and Rhodamine B, core–shell scaffolds treated with both dyes [Figure 6(A,B)] using simple adsorption displayed release percentages statistically similar to PCL–gelatin scaffolds treated with adsorption of one or both dyes.

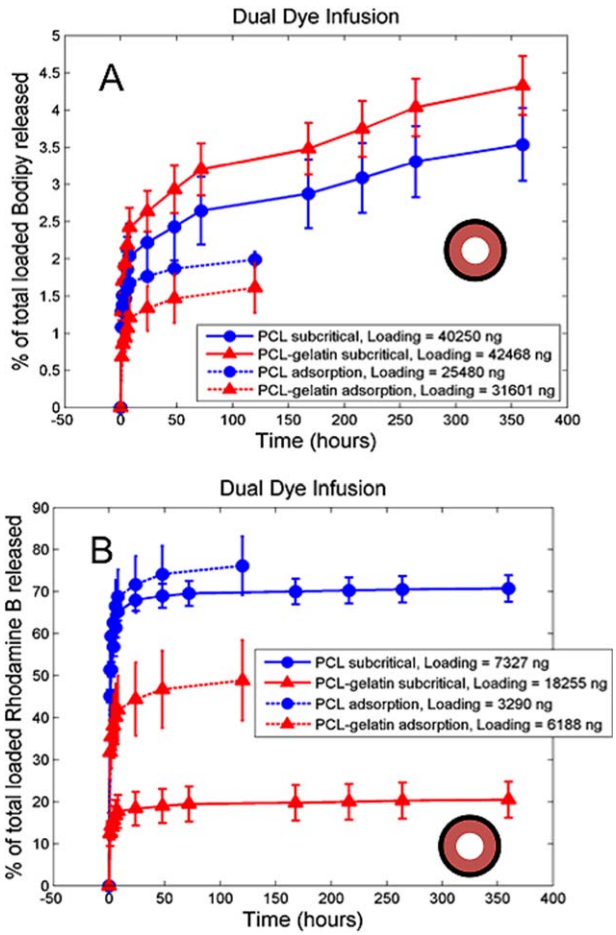

Figure 5. Release of A) BODIPY and B) Rhodamine B represented as a percent of initial scaffold loading following simultaneous infusion of both dyes into either PCL or PCL–gelatin. A representation of expected dye distribution through a fiber cross-section is given as an inset. Initial loading in nanograms is also given. Release of Rhodamine B from PCL following subcritical CO_2 infusion is nearly twice that observed in Figure 4(B), suggesting that addition of BODIPY to scaffold causes increased release of Rhodamine B. [Color figure can be viewed in the online issue, which is available at wileyonlinelibrary.com.]

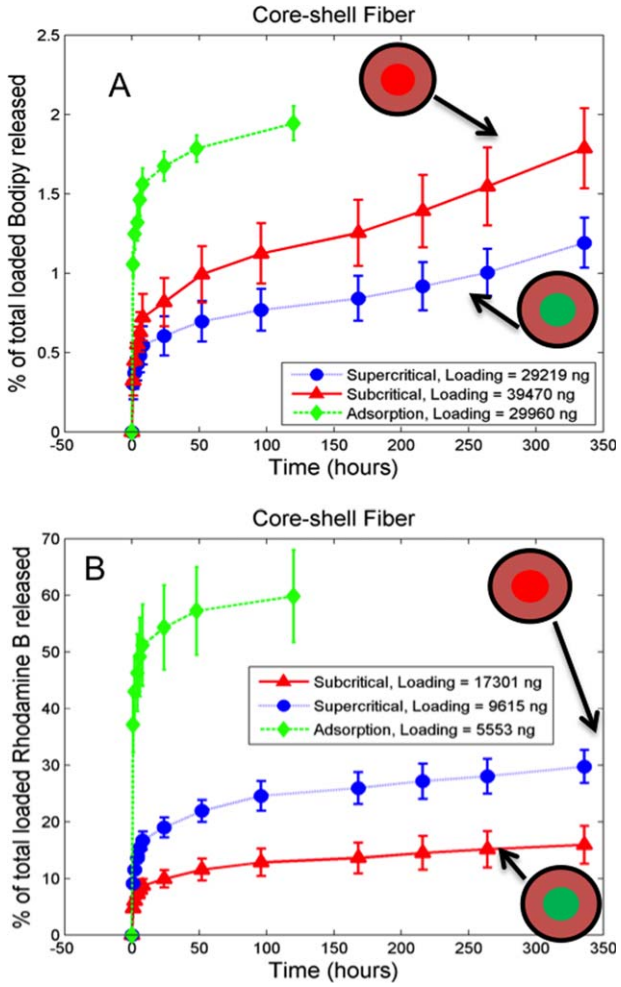

Figure 6. Release of A) BODIPY and B) Rhodamine B represented as a percent of initial scaffold loading following infusion into PCL "core" PCL–gelatin "shell" nanofibers using subcritical infusion, supercritical infusion, or simple adsorption conditions. A representation of expected dye distribution through a fiber cross-section is given as an inset. Initial loading in nanograms is also given. The percentage released following adsorption is very similar to that of Figure 5 as anticipated given that the exterior surface of the nanofiber is identical. [Color figure can be viewed in the online issue, which is available at wileyonlinelibrary.com.]

Previous literature suggests that stronger drug–scaffold interactions allows for slower, more linear release while either a negative or a lack of interaction promotes burst or rapid release.[43] In our results, BODIPY exhibited slow and limited release from all scaffolds, due to both a strong interaction with hydrophobic PCL domains found in all of the scaffolds studied as well as poor interactions with PBS as a release solvent. Rhodamine B, on the other hand, showed much faster release from hydrophobic PCL than hydrophilic PCL–gelatin as evidenced by Figures 4(B), and 5(B).

Dye Infusion and Loading Analysis

Hydrophilic–hydrophobic interactions between drug and scaffold should exert a profound but predictable effect on drug loading. To further corroborate evidence of the effects that hydrophobic–hydrophilic interactions have on drugs infused into nanofiber scaffolds via CO_2, differential loading of dyes was also quantified. Dye content for all scaffolds was on the order of 0.1% w/w. Figure 7(A) displays the total loaded BODIPY content in PCL or PCL–gelatin nanofiber scaffolds treated using either subcritical CO_2 or simple adsorption. Subcritical CO_2 infusion of BODIPY into PCL or PCL–gelatin scaffolds displayed significantly greater loading than adsorption, approximately a 30% increase. No significant differences in loading were observed between PCL and PCL–gelatin scaffolds [Figure 7(A)]. Similar trends were observed for BODIPY loading when both dyes were infused into PCL or PCL–gelatin scaffolds, resulting in a net 45% increase over simple adsorption. No significant differences were observed in the loading of BODIPY between single and dual dye adsorption. Figure 8 shows that supercritical infusion resulted in no significant differences in BODIPY loading compared to adsorption. Subcritical infusion of BODIPY resulted in a 33% increase in loading compared to adsorption.

Loading of Rhodamine B into PCL or PCL–gelatin scaffolds [Figure 7(A)] and into core–shell samples [Figure 7(B)] further

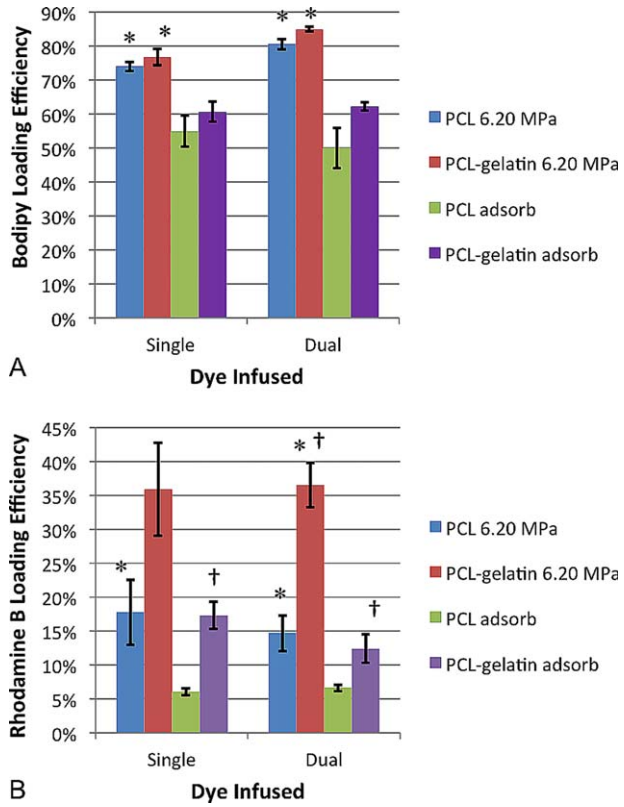

Figure 7. A) Absolute BODIPY loading into either PCL or PCL–gelatin. Subcritical CO_2 exposure increases dye loading over simple adsorption by ~50% for PCL and ~30% for PCL–gelatin. B) Absolute Rhodamine B loading into either PCL or PCL–gelatin under subcritical CO_2 conditions versus simple adsorption at 25°C. Subcritical CO_2 exposure increases dye loading over simple adsorption by ~300% for PCL and ~200% for PCL–gelatin. †Statistically different from pure-PCL adsorption condition ($p < 0.05$). *Statistically different from PCL-gelatin 6.20 MPa and adsorption ($p < 0.05$). [Color figure can be viewed in the online issue, which is available at wileyonlinelibrary.com.]

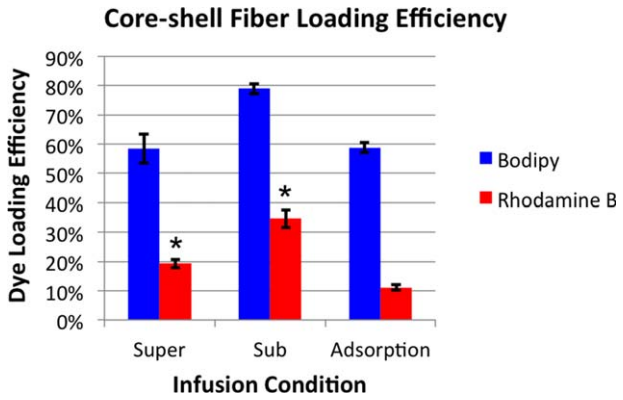

Figure 8. Absolute Rhodamine B (grey) and BODIPY (black) loading into PCL "core" PCL–gelatin "shell" nanofibers under subcritical (6.2MPa, 25°C) and supercritical (8.27 MPa, 37°C) CO_2 conditions versus simple adsorption at 25°C. Supercritical CO_2 exposure increases Rhodamine B loading by ~100% over simple adsorption and subcritical CO_2 exposure increases Rhodamine B loading by ~200% over adsorption. Supercritical CO_2 exposure does not result in any statistical difference of BODIPY loading into these scaffolds compared to adsorption. *Statistically different from adsorption condition ($p < 0.05$). [Color figure can be viewed in the online issue, which is available at wileyonlinelibrary.com.]

shows that significant improvements in loading were achieved when CO_2 infusion was utilized over adsorption. Subcritical CO_2 infusion resulted in nearly twofold increases in Rhodamine B loading compared to adsorption on hydrophilic PCL–gelatin. Nearly a threefold increase in loading over adsorption was achieved for Rhodamine B infused into hydrophobic PCL nanofibers by subcritical CO_2, suggesting that CO_2 infusion is especially capable of increasing loading for drugs and scaffolds with unfavorable interactions. Similar trends were observed for core–shell scaffolds [Figure 7(B)], showing a significant increase in loading for supercritical and subcritical infusion of Rhodamine B over simple adsorption.

We observed that dyes infused into favorable scaffolds exhibited high loading. Based on the high loading shown in Figures 7(A) and 8, BODIPY continues to interact somewhat favorably with a PCL–gelatin blend containing 50% hydrophobic PCL. Loading of BODIPY was significantly greater than loading of Rhodamine B under all conditions. This is reasonable as the wash solution used was 70% ethanol in water, a very hydrophilic mixture. This solvent was likely able to remove surface-bound Rhodamine B from the scaffold more effectively than BODIPY regardless of infusion conditions.

Almost twice as much Rhodamine B was loaded into scaffolds by infusion compared to adsorption. BODIPY was loaded on average 45% more effectively by subcritical infusion versus adsorption. CO_2 infusion accomplishes this by plasticizing PCL, enabling infusion of dye deeper into the polymer bulk. CO_2 infusion is therefore an effective tool to enhance and control drug–scaffold interactions within nanofiber scaffolds. Surprisingly, loading was found to be higher for dyes when subcritically infused into core–shell scaffolds versus supercritically infused. In its supercritical fluid phase, CO_2 may be dissolving and leaching dye from the scaffolds during infusion. This is plausible given the results of a study by Zhao *et al.*, which revealed increasing solubility of Rhodamine B with increasing pressure of CO_2, as well as an intrinsically high solubility of nonpolar dyes like BODIPY in supercritical CO_2.[44]

Interactions and CO_2 infusion in Core–Shell Scaffolds for Multidrug Release. Based on the results of this study, we hypothesize that the favorable intermolecular interactions of the hydrophobic PCL with BODIPY results in preferred partitioning of BODIPY within the PCL core. Similarly, the greater intermolecular interactions of the hydrophilic gelatin with Rhodamine B results in preferred partitioning of Rhodamine B within the PCL–gelatin shell. Using different phases of CO_2 can further modulate drug localization in core–shell nanofibers, providing facile control of loading and release behavior. Subcritical CO_2 infusion induces preferred partitioning into the superficial shell while supercritical CO_2 induces preferred partitioning into the core.

Figure 6 displays very slow, linear release when BODIPY is infused into a PCL core with supercritical CO_2 and when Rhodamine B is infused into a PCL–gelatin shell using subcritical CO_2. Infusing BODIPY into the shell or Rhodamine B into the core leads to faster release, while simple adsorption leads to a rapid initial burst of drug release. These observations suggest that supercritically infused BODIPY and subcritically infused Rhodamine B experience favorable interactions with the scaffold, while subcritically infused BODIPY and supercritically infused Rhodamine B experience relatively unfavorable interactions. Therefore, supercritical infusion likely infuses BODIPY into the hydrophobic core while the less penetrating subcritical infusion likely infuses Rhodamine B into the hydrophilic shell. These observations are consistent with the interaction-release relationship anticipated for these drug–scaffold combinations and validate that CO_2 infusion and drug–scaffold interactions can be effectively utilized to biofunctionalize electrospun nanofiber scaffolds and tailor the release profile of multiple biomolecules within such scaffolds.

Previous studies in our group[24,34] and others[45,46] have validated CO_2 infusion as a method for facile loading of molecules into polymer matrices and shown control of loading and release by altering process parameters such as pressure and phase of CO_2. This study identifies and characterizes an additional approach for controlled release in such systems based on hydrophilic–hydrophobic interactions between drug and scaffold. Through intelligent materials selection and scaffold design, these interactions can be leveraged to tailor loading and release performance, potentially allowing for scaffolds that elute two or more drugs with vastly different release profiles. Such a scaffold would be of great use as a drug delivery patch or tissue engineering scaffold.[47] Conceivably, a core–shell electrospun scaffold could be CO_2 infused with an antibacterial drug and a growth factor in such a way that the antibacterial is partitioned into the shell for fast release and the growth factor is partitioned into the core for long-term release. This particular system would be valuable in several active areas of research, including orthopedic coatings that simultaneously prevent infection and promote bone

growth[48] as well as chronic wound healing patches that can rapidly address infection while inducing angiogenesis over time.[49]

CONCLUSIONS

Electrospun nanofibers are promising materials for drug delivery and tissue engineering applications. CO_2 infusion technology can further augment nanofiber biomaterials by incorporating bioactivity through growth factors and other biomolecules. CO_2 infusion holds advantages over other methods for drug infusion in that it is an inexpensive, green, and bioactivity-preserving vector for impregnation. This study used dyes to provide a better understanding of the effects of hydrophobic–hydrophilic interactions within CO_2 infused nanofiber systems. This type of drug–scaffold interaction should be favorable in order to elicit long-term, linear release but unfavorable if the goal is to elicit rapid burst release of drug. CO_2 infusion provides an approach to engineer such interactions and achieve desirable release profiles by embedding different drugs within the nanofiber scaffold. In particular, biphasic core–shell nanofiber scaffolds can achieve an even greater level of control over release using different phases of CO_2 to partition drugs within composite scaffolds. Future work will capitalize on this high level of control to build a core–shell nanofiber scaffold capable of bimodal release of two biomolecules relevant to chronic wound healing.

ACKNOWLEDGMENTS

This work is supported by a research grant from the National Science Foundation under Grant No. EEC-0425626. This work is also supported by an undergraduate honors thesis scholarship from the Ohio State College of Engineering to BCG. Any opinions, findings, and conclusions or recommendations expressed in this material are those of the authors and do not necessarily reflect the views of the National Science Foundation or The Ohio State University.

REFERENCES

1. Gilchrist, T.; Martin, A. M. *Biomaterials* **1983**, *4*, 317.
2. Fraser, R.; Gilchrist, T. *Biomaterials* **1983**, *4*, 222.
3. Oliver, R.; Barker, H.; Cooke, A.; Grant, R. *Biomaterials* **1982**, *3*, 38.
4. Caiado, F.; Carvalho, T.; Silva, F.; Castro, C.; Clode, N.; Dye, J. F.; Dias, S. *Biomaterials* **2011**, *32*, 7096.
5. Mi, F.; Shyu, S.; Wu, Y.; Lee, S.; Shyong, J.; Huang, R. *Biomaterials* **2001**, *22*, 165.
6. Sudheesh Kumar, P. T.; Raj, N. M.; Praveen, G.; Chennazhi, K. P.; Nair, S. V.; Jayakumar, R. *Tissue Eng. Part A* **2013**, *19*, 380.
7. Biagini, G.; Bertani, A.; Muzzarelli, R.; Damadei, A.; Dibenedetto, G.; Belligolli, A.; Riccotti, G.; Zucchini, C.; Rizzoli, C. *Biomaterials* **1991**, *12*, 281.
8. Matouskova, E.; Broz, L.; Stolbova, V.; Klein, L.; Konigova, R.; Vesely, P. *Biomed. Mater. Eng.* **2006**, *16*, S63.
9. Drexler, J. W.; Powell, H. M. *Acta Biomater.* **2011**, *7*, 1133.
10. Zaari, N.; Rajagopalan, P.; Kim, S.; Engler, A.; Wong, J. *Adv. Mater.* **2004**, *16*, 2133.
11. Miller, R.; Brady, J.; Cutright, D. *J. Biomed. Mater. Res.* **1977**, *11*, 711.
12. Pan, H.; Jiang, H.; Chen, W. *Biomaterials* **2006**, *27*, 3209.
13. Reddy, V. J.; Radhakrishnan, S.; Ravichandran, R.; Mukherjee, S.; Balamurugan, R.; Sundarrajan, S.; Ramakrishna, S. *Wound Repair Regen.* **2013**, *21*, 1.
14. Khil, M.; Cha, D.; Kim, H.; Kim, I.; Bhattarai, N. *J. Biomed. Mater. Res. Part B* **2003**, *67B*, 675.
15. Leung, V.; Ko, F. *Polym. Adv. Technol.* **2011**, *22*, 350.
16. Sell, S. A.; McClure, M. J.; Garg, K.; Wolfe, P. S.; Bowlin, G. L. *Adv. Drug Deliv. Rev.* **2009**, *61*, 1007.
17. Rho, K.; Jeong, L.; Lee, G.; Seo, B.; Park, Y.; Hong, S.; Roh, S.; Cho, J.; Park, W.; Min, B. *Biomaterials* **2006**, *27*, 1452.
18. Truong, Y. B.; Glattauer, V.; Briggs, K. L.; Zappe, S.; Ramshaw, J. A. M. *Biomaterials* **2012**, *33*, 9198.
19. Shin, Y. M.; Shin, H.; Lim, Y. M. *Macromol. Res.* **2010**, *18*, 472.
20. Ji, W.; Yang, F.; van den Beucken, J. J. J. P.; Bian, Z.; Fan, M.; Chen, Z.; Jansen, J. A. *Acta Biomater.* **2010**, *6*, 4199.
21. Natu, M. V.; de Sousa, H. C.; Gil, M. H. *Stud. Mechanobiol. Tissue Eng. Biomater.* **2011**, *8*, 57.
22. Chen, F.; Zhang, M.; Wu, Z. *Biomaterials* **2010**, *31*, 6279.
23. Madurantakam, P. A.; Rodriguez, I. A.; Beckman, M. J.; Simpson, D. G.; Bowlin, G. L. *J. Bioact. Compat. Polym.* **2011**, *26*, 578.
24. Ayodeji, O.; Graham, E.; Kniss, D.; Lannutti, J.; Tomasko, D. *J. Supercrit. Fluids* **2007**, *41*, 173.
25. Sproule, T.; Lee, J.; Li, H.; Lannutti, J.; Tomasko, D. *J. Supercrit. Fluids* **2004**, *28*, 241.
26. Ginty, P. J.; Barry, J. J. A.; White, L. J.; Howdle, S. M.; Shakesheff, K. M. *Eur. J. Pharm. Biopharm.* **2008**, *68*, 82.
27. Sen, C. K.; Gordillo, G. M.; Roy, S.; Kirsner, R.; Lambert, L.; Hunt, T. K.; Gottrup, F.; Gurtner, G. C.; Longaker, M. T. *Wound Repair Regen.* **2009**, *17*, 763.
28. Losi, P.; Briganti, E.; Errico, C.; Lisella, A.; Sanguinetti, E.; Chiellini, F.; Soldani, G. *Acta Biomater.* **2013**, *9*, 7814.
29. Thakur, R. A.; Florek, C. A.; Kohn, J.; Michniak, B. B. *Int. J. Pharm.* **2008**, *364*, 87.
30. Jiang, B.; Zhang, G.; Brey, E. M. *Acta Biomater.* **2013**, *9*, 4976.
31. Xie, Z.; Paras, C. B.; Weng, H.; Punnakitikashem, P.; Su, L.; Vu, K.; Tang, L.; Yang, J.; Nguyen, K. T. *Acta Biomater.* **2013**, *9*, 9351.
32. Yoon, H.; Kim, G. *J. Pharm. Sci.* **2011**, *100*, 424.
33. Gaumer, J.; Prasad, A.; Lee, D.; Lannutti, J. *Acta Biomater.* **2009**, *5*, 1552.
34. Nelson, M. T.; Munj, H. R.; Tomasko, D. L.; Lannutti, J. J. *J. Supercrit. Fluids* **2012**, *70*, 90.
35. Verreck, G.; Decorte, A.; Li, H.; Tomasko, D.; Arien, A.; Peeters, J.; Rombaut, P.; Van den Mooter, G.; Brewster, M. E. *J. Supercrit. Fluids* **2006**, *38*, 383.
36. Gallego-Perez, D.; Higuita-Castro, N.; Sharma, S.; Reen, R. K.; Palmer, A. F.; Gooch, K. J.; Lee, L. J.; Lannutti, J. J.; Hansford, D. J. *Lab. Chip* **2010**, *10*, 775.

37. Heath, D. E.; Lannutti, J. J.; Cooper, S. L. *J. Biomed. Mater. Res. Part A* **2010**, *94A*, 1195.

38. Johnson, J.; Nowicki, M. O.; Lee, C. H.; Chiocca, E. A.; Viapiano, M. S.; Lawler, S. E.; Lannutti, J. J. *Tissue Eng. Part C-Methods* **2009**, *15*, 531.

39. Drilling, S.; Gaumer, J.; Lannutti, J. *J. Biomed. Mater. Res. Part A* **2009**, *88A*, 923.

40. Powell, H.; Kniss, D.; Lannutti, J. *Langmuir* **2006**, *22*, 5087.

41. Kull, K.; Steen, M.; Fisher, E. *J. Membr. Sci.* **2005**, *246*, 203.

42. Wang, Li-hong; Che, Xin; Xu, Hui; Zhou, Li-li; Han, Jing; Zou, Mei-juan; Liu, Jie; Liu, Yi; Liu, Jin-wen; Zhang, Wei; Cheng, Gang. *Int. J. Pharm.* **2013**, *454*, 135.

43. Zeng, J.; Yang, L.; Liang, Q.; Zhang, X.; Guan, H.; Xu, X.; Chen, X.; Jing, X. *J. Controlled Release* **2005**, *105*, 43.

44. Zhao, C.; Wang, J.; Tabata, I.; Hori, T. *Adv. Tex. Mater., Pts 1–3* **2011**, *332-334*, 146.

45. Hile, D. D.; Amirpour, M. L.; Akgerman, A.; Pishko, M. V. *J. Controlled Release* **2000**, *66*, 177.

46. Howdle, S.; Watson, M.; Whitaker, M.; Popov, V.; Davies, M.; Mandel, F.; Wang, J.; Shakesheff, K. *Chem. Commun.* **2001**, 109.

47. Browne, S.; Pandit, A. *J. Mat. Chem. B* **2014**, *2*, 6692.

48. Wenke, J. C.; Guelcher, S. A. *Exp. Opin. Drug Delivery* **2011**, *8*, 1555.

49. Boateng, J. S.; Matthews, K. H.; Stevens, H. N. E.; Eccleston, G. M. *J. Pharm. Sci.* **2008**, *97*, 2892.